Applied Acoustics 229 (2025) 110381

Contents lists available at ScienceDirect

Applied Acoustics

journal homepage: www.elsevier.com/locate/apacoust

Acoustic performance of multi-resonator screens in a virtually reconstructed open-plan office

Giulia Fratoni [a], Martin Tenpierik [b], Michela Turrin [b], Massimo Garai [a], Dario D'Orazio [a,*]

[a] Department of Industrial Engineering (DIN), University of Bologna, Italy
[b] Architectural Engineering and Technology Department, TU Delft, Netherlands

ARTICLE INFO

Keywords:
Wave-based simulations
Open-plan offices
Multi-resonator screens

ABSTRACT

Sound-absorbing barriers and screens are commonly employed to mitigate one of the most annoying noises in workplaces: intelligible speech. However, isolating their acoustic contribution from all the other elements (ceilings, wall treatment, or carpets) is challenging. This study uses a wave-based room acoustic modeling approach to explore the acoustic function of desk screens in a virtually reconstructed open-plan office. Analytical models, finite-element simulations, and experimental data from 3D-printed samples allowed defining a multi-resonator unit cell, attenuating the voice signal's main formants. The sound-absorbing panels composed of the unit modules iteration are assessed in the full-scale digital model, starting from the calibrated version on in-field measurements. The wave-based engine employed in this study grants the crucial aspect of computing the acoustic performance of the potential multi-resonator screens, including the edge diffraction due to their desk installation. In the virtual workplace, the acoustic role of such screens in increasing the speech level decay is outlined in comparison with the calibrated scenario and the traditional screens' option.

1. Introduction

Noise is a controversial aspect of working spaces such as open-plan offices. It can be beneficial when masking distractions, while detrimental when annoying employees and affecting task performance with unwanted sounds [1,2]. Generally, noise can be generated by external traffic, mechanical sources, and human-related sounds [3,4]. However, assuming properly insulated buildings and moderate levels of heating, ventilation, and air conditioning (HVAC) systems (below 40 - 45 dBA), the primary noise involves human activities, such as telephone rings, typing, footfall, and conversations [5,6]. Among these latter, studies identified intelligible speech as one of the most annoying and distracting factors decreasing work performance and overall job satisfaction [1,7,8]. For this reason, ISO 3382-3:2022 and ISO 22955:2021 standards adopt speech-related room acoustic criteria to describe the acoustic conditions in open-plan offices [9,10].

Along with many other variables, such as ceiling treatments, furniture ensembles, masking sounds, and zoning strategies, the open-plan offices' acoustic design frequently involves sound-absorbing screens/partitions, either between the workstations or directly on the workers' desks [11–14]. The consequent increase of the speech level decay throughout the space is closely related to their physical and acoustic features, such as their height, sound-absorbing, and sound-transmitting properties [15,16]. Table 1 offers a non-exhaustive list of references concerning screens in open-plan offices. For each study, the available data concerning the screens' features investigated (i.e., the height and the sound absorption) and the methods employed (i.e., analytical, experimental, and simulations) are reported. In a few cases, screens are not sound-absorbing, i.e., "unclassified" according to ISO 11654 [17], while most of the studies involve sound-absorbing screens. Traditional porous sound-absorbing screens are usually 3-5 cm thick panels with a structural board (or frame) combined with fabric upholstery. Sometimes transparent screens are preferred, e.g., glass, plexiglass, and micro-perforated glass partitions [18–20].

Distinguishing the screens' role from the other acoustic treatments, such as sound-absorbing ceilings, in reducing speech levels remains challenging. Ray-based algorithms - traditionally employed in room acoustic simulations - have inherent constraints in directly computing the sound diffracted by screens, especially at conversational distance. Therefore, the acoustic design of open-plan offices including screens would benefit from a wave-based approach to compute all the diffrac-

* Corresponding author.
E-mail address: dario.dorazio@unibo.it (D. D'Orazio).

https://doi.org/10.1016/j.apacoust.2024.110381
Received 5 June 2024; Received in revised form 9 October 2024; Accepted 31 October 2024
Available online 11 November 2024

Table 1
Screens' features investigated and models employed in previous studies (non-exhaustive list).

Reference	Screens' feature		Model		
	Height	Sound-absorption	Analytical	Experimental	Numerical
Keranen et al. 2023 [21]	×	×	×	×	×
Brawata et al. 2019 [18]		×			
Keranen et al. 2020 [15]	×	×		×	
Braat-Eggen et al. 2019 [22]	×				
Haapakangas et al. 2014 [23]	×				
Schmich et al. 2012 [24]	×	×		×	×
Balazova et al. 2008 [25]		×		×	×
Keranen et al. 2008 [19]	×	×		×	
Venetjoki et al. 2006 [26]	×				
Wang et al. 2002 [27]	×	×	×		
Wang et al. 2002 [28]	×	×	×	×	
Moreland 1988 [12]	×	×		×	
West et al. 1978 [13]	×			×	

tion effects caused by desk partitions in the near field, where the Fresnel-Kirchhoff approximation is no longer valid.

The present paper explores the increase of speech level decay due to screen installation in a virtually reconstructed open-plan office employing wave-based numerical methods. Analytical models inspired by previous literature and finite-element models allowed for designing multi-resonator (MR) unit cells to maximize the acoustic performance at mid frequencies (500 Hz - 1500 Hz), where the first two speech formants are defined [29,30]. The unit module thus obtained was manufactured with 3D printing technologies and then tested at the Delft University of Technology laboratories. First, the sound-absorbing properties of the 3D printed samples were assessed through impedance tube measurements. Then, the digital twin of an existing open-plan office - calibrated on measured room criteria - helped validate the overall acoustic function of desk partitions. The wave-based (WB) approach enabled the simulation of all the wave phenomena typically approximated by geometrical acoustics (GA) software. The enhancement in ISO 3382-3 and ISO 22955 metrics at individual workstations are evaluated for the proposed MR partition and traditional solutions (porous and glass panels).

2. The multi-resonator (MR) unit module

The present section reports the analytical hints and the finite-element models used to design the unit module of the proposed sound-absorbing panels.

2.1. Preliminary design choices

In the present study, the choice of the sound-absorbing behavior fell on the Helmholtz resonance due to the high adaptability to absorb sound energy at specific frequency ranges exploiting resonators' dimensions. In detail, the neck-embedded Helmholtz resonators have been used instead of classical Helmholtz resonators to maintain reasonable sample thicknesses [31]. Existing analytical models inspired the mathematical implementation to find the total acoustic impedance of each resonator as the sum of the cavity impedance, the neck impedance, and specific correction factors [32–34].

The acoustic impedance of the cavity Z_c can be expressed as:

$$Z_c = -j\frac{S_c \rho_c c_c^2}{\omega V} \tag{1}$$

with $S_c = \pi(d_c/2)^2$ the inner area of the cavity, $\rho_c = \rho_0/\Psi_v$, $c_c = \omega/k_c$, k_c is the wave number, ω is the angular frequency, V is the volume of the irregular chamber, and

$$k_c = k_0\sqrt{\frac{\gamma_{air} - (\gamma_{air}-1)\Psi_{h,c}}{\Psi_{v,c}}}. \tag{2}$$

The functions

$$\Psi_{h,c} = \frac{J_2(k_h(d_c/2+b))}{J_0(k_h(d_c/2+b))} \tag{3}$$

and

$$\Psi_{v,c} = \frac{J_2(k_v(d_c/2+b))}{J_0(k_v(d_c/2+b))} \tag{4}$$

are referred to as the thermal and viscous fields inside the cavity, where J_2, J_0 are the Bessel functions of order two and zero respectively, $k_h = \sqrt{-j\omega(\rho_0 C_p/K)}$ is the thermal wave number, and $k_v = \sqrt{-j\omega(\rho_0/\eta)}$ is the viscous wave number (with η as the dynamic viscosity of air). The acoustic impedance of the neck Z_n considering the thermal losses is defined as:

$$Z_n = \frac{-j\rho_0\omega l_n}{\Psi_{v,n}} \tag{5}$$

where $\Psi_{v,n} = J_2(k_v d_n/2)/J_0(k_v d_n/2)$ is the function of viscous field inside the neck and l_n the length of the neck.

The total acoustic impedance of the neck-embedded resonator Z is calculated as:

$$Z = \frac{A}{S_n}(Z_n + Z_c + 2\sqrt{2\omega\rho_0\eta} + i\omega\rho\delta_i) \tag{6}$$

where $A = \pi(d_c/2+b)^2$ is the whole frontal area of the sample including the wall thickness b, $S_n = \pi(d_n/2)^2$ is the area of the neck, and $2\sqrt{2\omega\rho_0\eta} + i\omega\rho\delta_i$ are the end corrections. In detail, $\delta_i = [1 + (1 - 1.25\epsilon)](4/3\pi)d_n$ is the end correction of the acoustic mass resulting from the wave radiation ($\epsilon = d_n/d_c$), and the additional term $2\sqrt{2\omega\rho_0\eta}$ is due to frictional losses caused by air flow along the boundaries of the neck. From Eq. (6) the normal incidence sound absorption coefficient, α_n, is the following:

$$\alpha_n = 1 - \left|\frac{Z - \rho_0 c_0}{Z + \rho_0 c_0}\right|^2 \tag{7}$$

where $\rho_0 c_0$ is the characteristic impedance of air.

Combining different resonators can maximize the normal incidence sound absorption coefficients in the frequency range interested by the voice signal spectrum [9,35]. Moreover, the need to geometrically arrange the required neck-embedded resonators in cylindrical samples with a diameter of 100 mm, i.e., the impedance tubes' size, entailed a 3D modeling process to choose each resonator's dimensions (see Fig. 1).

2.2. Sound absorption prediction through finite-element models

A virtual ISO 10534-2 measurements scenario was recreated within COMSOL Multiphysics through 3D meshes [36,37]. This step allowed finding adequate trade-offs between the measurement equipment's geometrical constraints and the required sample's sound-absorbing properties. The whole system involved the geometry of the potential sample

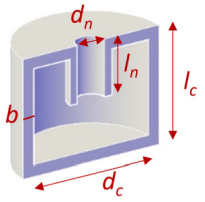

Fig. 1. 3D section of the single neck-embedded resonator. Main dimensional features are d_c, l_c, d_n, l_n, and b (see Sec. 2.1).

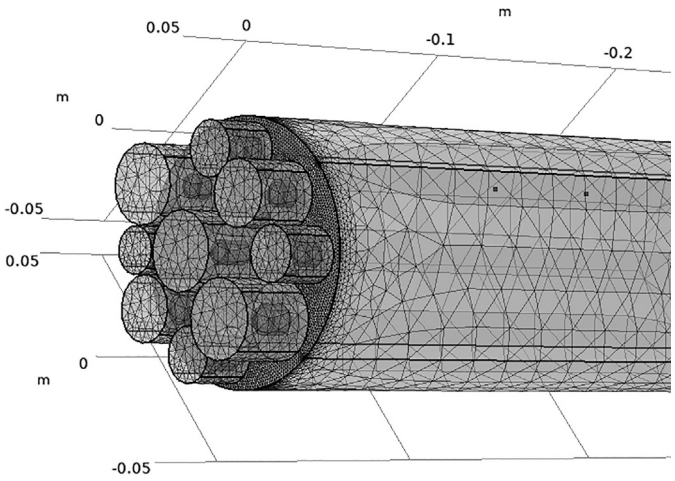

Fig. 2. Details of the input meshes built in the *Pressure acoustics, frequency domain* module of the FE model: air volumes corresponding to the resonators and the impedance tube (100 mm as diameter).

and the impedance tube (600 mm as overall length, 100 mm as diameter), in line with previous works involving finite-element (FE) simulations for resonator arrays [31,38]. The input mesh of the numerical model included ten different domains: the inner volumes within the nine resonators (air properties) and the air volume of the impedance tube (air properties, plane wave radiation), as depicted by Fig. 2. A minimum element size of the mesh was imposed to obtain at least six elements for the wavelength corresponding to the maximum frequency of 2000 Hz ($\lambda = 0.17$ m), according to convergence recommendations [39]. The FE model is excited at the tube's inlet boundary (loudspeaker) by a plane wave with a sound pressure amplitude of 1 Pa. The tube's lateral surfaces and the rear of the specimen were handled with hard boundary conditions, imposing null displacements along the tube's axial direction. Two points corresponding to the microphone positions allowed deriving the normal incidence sound absorption coefficient α_n as a function of the frequency through the transfer function expressions in ISO 10534-2 [36,40,41].

2.3. 3D printed samples

The analytical and numerical prediction models led to nine neck-embedded resonators fitting in a single sample, with distinct dimensional features' combinations (see Fig. 3(a)). Table 2 provides the resulting:

- diameters of each cavity, d_c (from 18 mm to 30 mm),
- lenghts of each cavity, l_c (from 18 mm to 30 mm),
- diameters of each neck, d_n (from 7 mm to 9 mm),
- lenghts of each neck, l_n (from 7 mm to 12 mm),

referring to the terminology used in previous studies and shown in Fig. 1.

The need for quickly manufactured prototypes required adopting 3D printing techniques. Such technologies are widely used in the engineering research community to design complex geometries that would otherwise be challenging with traditional manufacturing techniques [42]. 3D-printed samples enabled the authors to perform acoustic measurements to validate the analytical and numerical processes.

Table 2
Multi-resonator (MR) module's dimensional features (see Figs. 1 and 3): d_c and l_c are the diameters and the lengths of each cavity, while d_n and l_n are the diameters and the lengths of each neck.

	1	2	3	4	5	6	7	8	9
d_c (mm)	30	30	30	25	25	21	21	21	18
l_c (mm)	30	30	30	25	25	21	21	21	18
d_n (mm)	7	7	9	7	9	7	8	9	7
l_n (mm)	12	7	9	7	9	7	8	9	7

The first technology is fused deposition modeling (FDM), a widely used 3D printing technique involving the deposition of melted thermoplastic polymers in a predetermined path to form the final object. FDM is one of the most popular and widespread additive manufacturing technologies because of its affordable costs and the wide variety of thermoplastic polymers that can be used [43]. The material selected is MakerPoint PLA Natural, a biobased Polylactic Acid (PLA), for its mechanical properties, such as high tensile modulus, strength, transparency, and sustainability. The Ultimaker 3 printer at the Delft University of Technology Labs allowed for manufacturing the FDM specimen, with a total thickness of 33 mm [44]. The finest setups were chosen in terms of the minimum printing speed (30 mm/s) and minimum layer height (0.1 mm) [45]. The prototype has been printed in two components for practical reasons and then glued together (see Fig. 3(b)).

The second technology is the stereolithography (SLA) technique, which creates 3D objects through photopolymerization. Such a process, known for its high precision and resolution, is usually used to produce intricate and highly detailed objects with smooth surfaces. SLA supports a variety of materials, but resins are the most widely employed and tailored materials for specific applications. The DWS XFAB 2000 SLA 3D printer at the University of Bologna and the INVICTA 977 resin have been employed during this step. This photosensitive material is explicitly suitable to high-definition functional prototypes with stereolithography 3D printers (see Fig. 3(c)). It is long-lasting, resistant, and slightly flexible. The thickness of the overall resin specimen is approximately 33 mm. The authors selected semi-transparent materials for both 3D printing technologies to moderate the barrier effect to sight and light at the workstations - typical of opaque panels installations - without undermining the workers' visual privacy.

2.4. Experimental outcomes

Measurements of normal incidence sound absorption coefficient (α_n) were carried out for both specimens shown in Figs. 3(b) and 3(c). The first specimen was tested at the Delft University of Technology using the Brüel & Kjær impedance tube kit type 4206 (700 mm as overall length, 100 mm as diameter, range 50 - 1600 Hz). During the measurements, the recorded thermo-hygrometric conditions showed the temperature equal to 22 °C and the relative humidity at 40%. The resulting trend of α_n is the average of three measurements performed on the FDM specimen. The second specimen was tested at the University of Bologna through a custom impedance tube complying with ISO 10534 (600 mm as overall length, 100 mm as diameter, range 300 - 4400 Hz). During the measurements, the recorded thermo-hygrometric conditions showed the temperature equal to 20 °C and the relative humidity at 50%.

Fig. 4 reports the numerical and measured α_n plots against the frequency. The match between these set of values is here assessed by comparing the peak's frequency (f_{max}) corresponding to each maximum α_n value. 94% of the percentage differences between numerical and measured α_n are below the 2% of the predicted values. Among this majority, 62% of the percentage differences are even lower than the 1.2% of the predicted values. The highest percentage discrepancies are encountered

(a) Multi-resonator (MR) unit module (b) Polylactic Acid (PLA) sample (c) Resin sample

Fig. 3. On the left, the layout of the multi-resonator (MR) unit module (nominal features in Table 2). In the center, the Polylactic Acid (PLA) sample printed through fused deposition modeling (FDM) techniques. On the right, the resin sample printed through stereolithography (SLA) techniques.

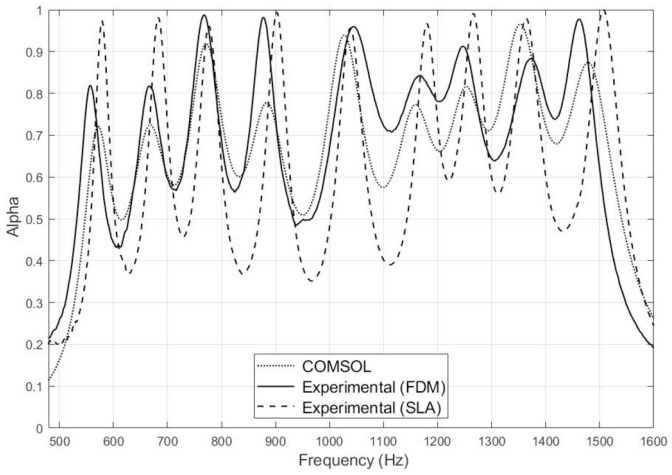

Fig. 4. Comparison between numerical (FE model within COMSOL) and measured α_n outcomes obtained with impedance tubes. MR module's geometrical data are provided in Table 2.

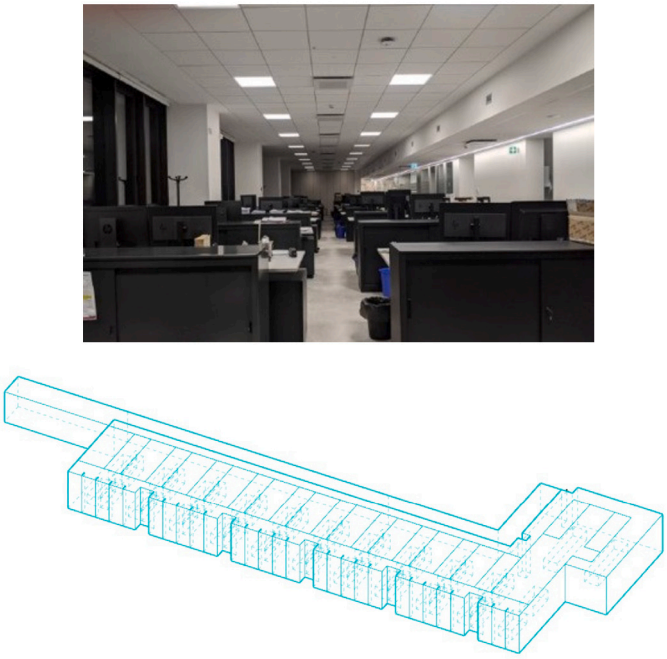

Fig. 5. At the top, a view of the open-plan office used as an existing reference to calibrate the virtually recreated scenario (photo taken by the authors). At the bottom, a view of the corresponding 3D model in SketchUp software (freely available at [46]).

for the FDM specimen at low frequencies (4.1% and 3.3% for resonator n. 1). In contrast, both specimens give the highest absolute differences (up to 25 and 28 Hz) at high frequencies (resonator n. 9 at around 1500 Hz). For the remaining peaks (from resonator n. 2 to resonator n. 8), there is a satisfactory match between prediction trends and the experimental outcomes on both 3D-printed specimens (percentage differences from 0.2% to 1.9%).

3. Screens' acoustic role in a virtually reconstructed scenario

The authors chose an existing open-plan office to assess the acoustic effect of potential MR screens when installed in a real-scale plausible scenario. Their contribution has been quantified and compared with the starting configuration without screens and traditional screen solutions through wave-based techniques.

3.1. The open-plan office

The environment selected for this work is a recently built open-plan office with a floor area of approximately 250 m^2 (7.5 x 33 m). As depicted in Fig. 5, the room (3 m high) shows a geometrical disproportion, and thus, the sound field could be assumed as anisotropic. Hence, the use of ISO 3382-3 is key in describing the spatial speech level decay through single-number values, i.e., $D_{2,S}$, $L_{p,A,S,4m}$, and r_c. The office hosts 26 workstations (around 10 m^2 for each workstation) with "small amount of collaborative work" according to ISO 22955 [10]. The distance between workstation islands is about 3 m, and the height of the storage units between them (1 m) does not influence the spatial sound decay throughout the environment (seated workers' mouths and ears at 1.2 m above the floor). The false ceiling of the open-plan office combines porous (mineral fiber) and perforated gypsum tiles. It is crucial to note that the office lacks effective sound screens, barriers, or partitions higher than 1.2 meters, either on or between the workstations. This workplace, with two corridors (1.2 m wide each) and no carpet on the floor, could be an exemplary outcome of a standard design approach lacking acoustic optimization, except for the ceiling treatment. For this reason, it represents a helpful starting point for assessing the installation of the MR screens and their assessment through numerical models.

Acoustic measurements were carried out to derive the spatial decay of A-weighted sound pressure level. The measurements were performed using pink noise, a custom high-SPL dodecahedron, and an NTI Audio MA220 microphone preamplifier. The microphone was moved in seven positions along a line path over the workstations, while the omnidirectional sound source was placed at one end of the measurement path [47]. The experimental ISO 3382-3 criteria were extracted from such in-field measurements [9].

Table 3
Boundary conditions assigned to the 3D model's surfaces. The wave-based part of the algorithm converts the frequency-dependent absorption coefficients α_{random} into complex acoustic impedances, while the ray-based part of the algorithm directly employs the absorption coefficients α_{random} and the scattering coefficients s given.

Materials	α_{random}							s
	125 Hz	250 Hz	500 Hz	1000 Hz	2000 Hz	4000 Hz	8000 Hz	
Floor	0.02	0.02	0.03	0.03	0.04	0.04	0.04	0.05
Walls (plasterboard)	0.15	0.16	0.15	0.13	0.12	0.10	0.10	0.05
Windows	0.11	0.10	0.09	0.09	0.09	0.09	0.09	0.05
Furnishing	0.06	0.09	0.15	0.20	0.20	0.10	0.10	0.30
Porous ceiling tiles	0.41	0.63	0.86	0.94	0.90	0.60	0.60	0.05
Perforated ceiling tiles	0.73	0.81	0.83	0.82	0.79	0.70	0.60	0.15
Glass screens	0.08	0.07	0.06	0.06	0.05	0.05	0.05	0.20
Porous screens	0.37	0.81	0.83	0.82	0.79	0.70	0.60	0.10
MR screens	0.18	0.32	0.76	0.84	0.37	0.20	0.18	0.20

3.2. Wave-based simulations setup

In the latest decades, wave-based simulation methods have been increasingly applied to room acoustics scenarios due to technological and numerical advances reducing computational time [48,49]. For this reason, they are becoming popular also in large-scale room acoustics simulations [50–54].

In wave-based room acoustic simulations, broad geometrical simplifications are not recommended, such as modeling a single box as the whole audience area. Instead, it is essential to ensure that the imported 3D model contains sufficient detail to predict the room's impulse response accurately. On the other hand, detail reduction and geometrical approximation are necessary to decrease computational time [55,56]. During the 3D modeling phase of the present work, best practice rules were followed, pursuing the best trade-off between physical accuracy and computational time:

- the air gap between the suspended and structural ceiling was not modeled;
- no details smaller than 0.1 m was modeled;
- each desk-seat pair was modeled as a single box;
- bookshelves between workstations were modeled as boxes.

The 3D virtual model of the open-plan office was built through Sketchup software version 2022 (see Fig. 5). A reduced number of tags allowed for sorting the surfaces (around 1250 m^2 as total area) into the main room elements: floor, walls, windows, furnishing, and ceiling (see Table 3).

After the 3D modeling step, the model was imported into the Treble Acoustic simulation suite [57]. The simulation algorithm employs a direct numerical wave equation solution in the time domain for low frequencies. The solver utilizes the discontinuous Galerkin (DG) method, specifically optimized for massively parallel high-performance computing clusters using graphics processing units (GPUs). The partial differential equations system, describing the acoustic wave propagation in a three-dimensional space, is numerically solved with the finite element approach by a high-order discretization in time and space to iteratively yield a solution [49]. Boundary conditions must be supplied in terms of complex, frequency-dependent surface impedances, which are typically derived from measurements or material analytical models. Moreover, a Geometrical Acoustics (GA) solver computes the high-frequency part of the acoustic response. In detail, the initial specular reflection reflections are calculated using a pressure-based Image Source Method (ISM), while the scattered energy from the first reflections and the latter portion of the energy histograms are calculated through the Ray-Radiosity (RR) method. The RR method provides energy histograms per octave band, which are processed into an impulse response. Then, they are combined with the ISM result to create the ray-based impulse response. The hybridization process in the frequency domain combines wave-based and ray-based results to create a broadband impulse response. According to the selected transition frequency (TF), a low-pass filter is applied to the wave-based solution to eliminate frequencies above TF, and a high-pass filter is applied to the geometrical acoustics solution to eliminate frequencies below TF. After a calibration of the output (94 dB at one meter from an omnidirectional point source in a free field), the filtered impulse responses are summed to produce the hybrid response. In the present study, the TF between the wave solver and GA was imposed equal to 1410 Hz, granting the direct computation of diffraction phenomena for most of the frequency range of interest for the MR unit module's absorption coefficient trend (see Fig. 4). With an office volume of 750 m^3, and a measured reverberation time of 0.69 s (the value averaged over the octave bands from 125 Hz to 8000 Hz), the TF chosen for the simulations setting is around 20 times higher than the room's Schroeder frequency, which is around 60 Hz [58]. Considering that the computation time is proportional to the volume (linearly), the reverberation time (linearly), and the highest frequency handled through the wave-based approach (with the power of four), each simulation took around 3 hours and 20 minutes.

The authors assigned boundary conditions to the model's surfaces from the list of materials in the software, scientific literature, and the technical data of the products installed in the open-plan offices (suspended ceiling tiles). While the ray-based model directly employs the energy-based α_{random} values, the wave-based approach needs conversion into pressure-based complex boundary conditions [59,60]. The non-unique retrieving process starts from the α_{random} values (provided by the user) and a surface impedance model, such as rigid, porous, and perforated panels. The goal is obtaining the random incidence absorption coefficient, $\bar{\alpha}$, computed from the surface impedance model:

$$\bar{\alpha} = \int_0^{\pi/2} \frac{\sin(2\theta)4\mathrm{Re}(Z)\cos(\theta)}{|Z|^2\cos\theta^2 + 2\mathrm{Re}(Z)\cos(\theta) + 1}\mathrm{d}\theta \tag{8}$$

where Z is the acoustic impedance and θ is the incidence angle. This can be done by minimizing a function m expressed as:

$$m = |\bar{\alpha} - \alpha_{random}| \tag{9}$$

with α_{random} the input absorption data. Then, auxiliary differential equations at the domain boundaries allow for obtaining the complex reflection factor R from the acoustic impedance Z:

$$R = \frac{Z-1}{Z+1}. \tag{10}$$

For the ray-based model, higher scattering values (s = 0.3) were assigned to the furniture and storage units in the room to compensate for the modeling approximation, according to literature [61]. A scattering value of s = 0.15 was applied to the perforated ceiling tiles. In contrast,

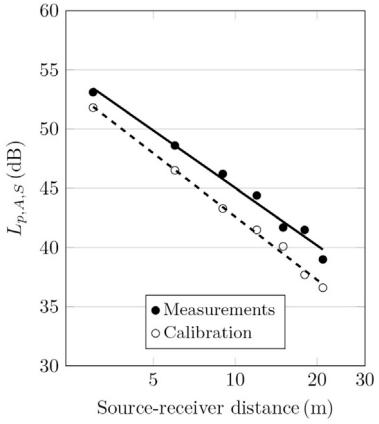

Fig. 6. Calibration outcomes (without screens): measured and simulated $L_{p,A,S}$ against the distance from the sound source [9].

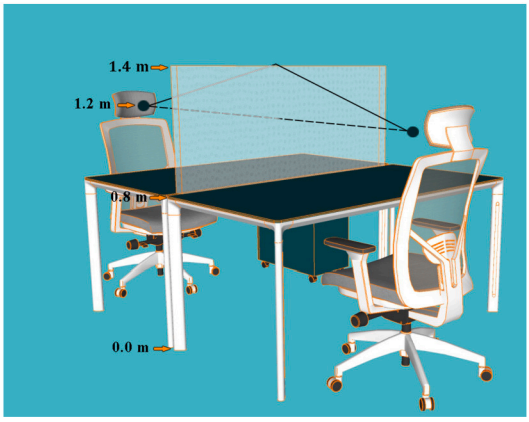

Fig. 7. View of a potential MR desk screen achieving the overall height of 1.40 m above the floor.

the standard value s = 0.05 was assigned to the remaining surfaces. All the sound absorption (α) and scattering (s) coefficients used are reported in Table 3. In the GA solver, the impulse response length and the number of rays were equal to 1500 ms and 40000 rays, respectively.

3.3. 3D model calibration

The 3D model was calibrated based on the experimental outcomes of ISO 3382 measurements in the configuration with no screens. $D_{2,S}$ was chosen as the reference metric, as it is an overall room property quantifying the decrease of the A-weighted SPL of speech by doubling the distance to the source. The calibration process involved a slight refinement of input data assigned to the surfaces within reliable ranges for each material: Table 3 reports the resulting boundary conditions [55,62]. Simulations were run until the difference between measured and simulated $D_{2,S}$ values was 0.1 dB. This value is lower than the $D_{2,S}$ measurements uncertainty according to previous studies (0.5 dB) [21,63] and the reproducibility standard deviations s_R provided by ISO 3382-3 (0.3 dB). Indeed, 0.5 and 0.3 dB refer to measurements in different systems (reproducibility), while simulation iteration is closer to the repeatability within the same system. However, these values can be considered plausible references for the tolerance ranges during the calibration process.

Fig. 6 shows the measured and simulated $L_{p,A,S}$ values at the workstations of the measurements linear path. $D_{2,S}$ value identifies the slope of each regression line. Concerning the $L_{p,A,S,4m}$ single-number value in the calibrated scenario, the measured and numerical values differ by 1.7 dB, a value reasonably comparable to the s_R of the single number values provided by ISO 3382–3 (1.1 for $L_{p,A,S,4m}$) [21,63–65]. The near field's influence on $L_{p,A,S,4m}$ values justifies a higher level of uncertainty, e.g., up to 2 dB (see the vertical shift in Fig. 6). In the same scenario, the discrepancy between measured and simulated r_c values is 1.3 m, corresponding to 16% of the measured value. Such difference is within 1.5 m [63] and also within the comfort distance's s_R values (21% for r_c) reported by ISO 3382-3.

3.4. MR screens' acoustic performance

After having tuned the virtual model on the experimental data, the authors assessed three simulated scenarios, adding different desk screens to increase $D_{2,S}$ and decrease $L_{p,A,S,4m}$ and r_c:

- transparent glass panels,
- traditional porous panels,
- the proposed panels with MR unit module arrays.

Table 4
Comparison between measured and simulated ISO 3382-3 metrics: $D_{2,S}$ (dB), $L_{p,A,S,4m}$ (dB), and r_c (m). The starting scenario gives the measured criteria in the open-plan office without screens. The calibrated scenario returns data from the digital twin tuned on the measured $D_{2,S}$ value (0.5 dB as tolerance range). The last three scenarios correspond to the virtual installation of glass, porous, and MR screens on the workers' desks, respectively.

Scenarios		$D_{2,S}$ (dB)	$L_{p,A,S,4m}$ (dB)	r_c (m)
Without screens	Measurements	5.9	50.8	7.9
	Calibration	5.8	49.1	6.6
With screens	Glass screens	6.5	47.9	5.4
	Porous screens	6.7	47.1	5.0
	MR screens	7.1	46.9	4.8

The height of each screen was set to achieve 1.4 m above the floor as overall height: 0.8 m (desk) and 0.6 m (screen). Fig. 7 shows two workstations with the screen installed on the desks. The MR screens comprise unit module iteration on both sides of each panel.

The random incidence sound absorption coefficients α_{random} of MR screens were estimated from measurement results obtained with impedance tubes. First, Annex E of ISO 10534-2 allowed for deriving α_{random} from the normalized impedance [36]. Then, the calculated values became the input data for the boundary conditions in the room acoustics simulator: α_{random} is the starting point for deriving the complex reflection factors in the wave-based engine. At the same time, they are directly assigned to surfaces in the ray-based approach. Acoustic properties of each partition type are provided in the last three rows of Table 3.

Table 4 shows the comparison between measured and simulated ISO 3382-3 metrics ($D_{2,S}$, $L_{p,A,S,4m}$, and r_c) related to the calibrated model and the three distinct scenarios assessed: glass, porous, and MR screens applied on workers' desks. All the desk screens help increase the speech level decay since they work as acoustic barriers between frontal workstations. Therefore, all the scenarios involving screens contribute to increasing $D_{2,S}$ and decreasing $L_{p,A,S,4m}$, and r_c. However, some slight differences exist in the three assessed scenarios listed hereafter.

- Glass screens contribute to increasing $D_{2,S}$ by 0.7 dB while porous screens by 0.9 dB from the calibrated configuration: from 5.8 dB to 6.5 dB and 6.7 dB, respectively. MR screens produce a $D_{2,S}$ increase of 1.3 dB from the calibrated scenario: from 5.8 dB to 7.1 dB.
- Similarly, glass screens reduce $L_{p,A,S,4m}$ by 1.2 dB while porous screens by 2.0 dB from the calibrated setting (from 49.1 dB to 47.9 dB and 47.1 dB, respectively). In the case of MR screens, $L_{p,A,S,4m}$ decreased by 2.2 dB from the calibrated scenario (from 49.1 dB to 46.9 dB).

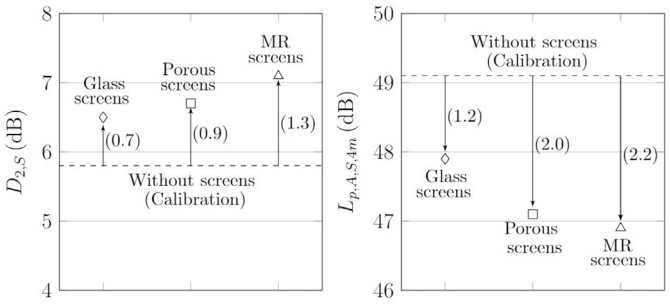

Fig. 8. Simulated scenarios with different screen types starting from the model without screens calibrated on experimental data. The effects on $D_{2,S}$ and $L_{p,A,S,4m}$ criteria are provided between brackets for each type of screen: glass screens, porous screens, and multi-resonator (MR) screens.

- Starting from $r_c = 6.6$ m in the calibrated model, glass screens cause a drop by 1.2 m, porous screens by 1.6, and MR screens by 1.8 m.

Fig. 8 highlights the effect of each screen choice on $D_{2,S}$ and $L_{p,A,S,4m}$ starting from the model without screens calibrated on experimental data. Since the differences between simulated outcomes are below 0.6 dB for $D_{2,S}$, and 1.0 dB for $L_{p,A,S,4m}$, all the evaluated configurations could be deemed equivalent solutions, also considering the simulations' uncertainty.

Numerical outcomes suggest MR screens as a potential solution for improving the ISO 3382-3 metrics. Moreover, given the plausible simulated results, the numerical method proves to be a feasible tool to predict the acoustic effect of non-traditional screens in open-plan offices. Finally, it is worth noting that the semi-transparent materials employed for the unit cells of the proposed MR screens (PLA filament and resin) could also simultaneously enhance acoustic and visual comfort, similarly to previous works employing transparent microperforated panels [20,66].

3.5. Limitations of the work

To better understand the potential applicability of the findings, the present section describes the factors that may affect their reliability or generalizability.

Simplification of variables. Indeed, comprehensive acoustic treatments of open-plan offices also address several more factors beyond screens, such as ceiling surfaces, furnishings, office etiquette, and sound masking [1]. Moreover, non-speech annoyance components in workspaces with a broadband signal are not negligible, such as typing and footfall [2,3]. However, the scope here is focusing on one of the most distracting noises, i.e., intelligible speech, and attempting to isolate the screens' acoustic role through wave-based simulations, similar to previous works based on measurement campaigns [15].

Choice of analysis method. The frequency range of measured data for the MR unit cell is limited to 500 - 1500 Hz due to practical constraints of the equipment and materials involved (impedance tube and sample with 100 mm as diameter). Furthermore, data may also suffer from inaccuracies or biases when converting the normal incidence to random incidence sound absorption coefficients and then retrieving the complex reflection factor needed as boundary conditions in the discontinuous Galerkin finite-element method [59,60]. However, the main objective of the work is to validate a prediction method rather than proposing a new partition for open-plan offices. The plausible MR screens' acoustic performance, comparable to glass and porous screens, proves wave-based models to be a potential prediction tool for estimating the influence of non-traditional screens on workspaces' acoustic metrics. Future works may involve full-scale screens to acquire broadband random incidence sound absorption data, carry out measurements in real-world scenarios, and investigate perceptual improvement through subjective tests.

4. Conclusions

This paper investigates the acoustic performance of MR desk partitions in a virtually reconstructed open-plan office, starting from a calibrated scenario without any screens. First, an MR unit module with nine neck-embedded Helmholtz resonators has been designed using analytical models and FE simulations. The geometrical features of each neck (d_n, l_n) and cavity (d_c, l_c) were optimized to maximize the sound-absorbing properties in the frequency range most interested by the prominent formants of voice signals ($\alpha_n > 0.5$ from 500 Hz to 1500 Hz). Acoustic measurements conducted on two semi-transparent 3D-printed samples (100 mm as diameter, 33 mm as thickness) through laboratory impedance tubes validated the design process of the unit cell: the percentage differences between experimental and numerical values proved to be below 2% of the predicted values for 94% of the cases (peaks' frequencies).

Then, a full-scale digital workplace scenario with a wave-based approach allowed for isolating the MR screen acoustic contribution from all the surrounding acoustic factors, e.g., the sound-absorbing treatments at the ceiling. The 3D model of an existing workplace was first calibrated on ISO 3382-3 measurement results in a reference configuration lacking acoustic partitions. The calibrated model was used as a starting point to estimate the proposed screens' acoustic role, along with traditional partitions (glass and porous screens). The transition frequency value between the discontinuous Galerkin FEM and the ray-tracing engine - set equal to 1410 Hz in each simulation - grants a higher level of accuracy in computing the diffracted sound in the near field, overcoming the typical constraints of classical room acoustics simulations approaches.

Results highlight that introducing screens into an acoustically treated office increases $D_{2,S}$ by 0.7 - 1.3 dB, decreases $L_{p,A,S,4m}$ by 1.2 - 2.2 dB, and r_c by 1.2 - 1.8 m. In detail, the MR screens returned enhancements in spatial decay metrics (a rise of 1.3 dB for $D_{2,S}$, a drop of 2.2 dB for $L_{p,A,S,4m}$ and 1.8 m for r_c), comparable to the simulated scenario with porous screens. From this preliminary evaluation based on numerical models, the proposed MR screens ad hoc designed to deteriorate voice signal could facilitate the achievement of the ISO 22955 target for "small amount of collaborative work" ($D_{2,S} > 7$ dB, $L_{p,A,S,4m} < 47$ dB) and to get closer to ISO 3382-3 recommendations ($D_{2,S} > 8$ dB, $L_{p,A,S,4m} < 48$ dB, and $r_c < 5$ m), increasing spatial decay of speech level throughout the space.

Materials employed in the present work, including the 3D model, the boundary conditions, and the outcomes of the measurements are available in an accessible online repository [46].

CRediT authorship contribution statement

Giulia Fratoni: Writing – review & editing, Writing – original draft, Visualization, Validation, Software, Methodology, Investigation, Formal analysis, Data curation, Conceptualization. **Martin Tenpierik:** Resources, Supervision. **Michela Turrin:** Resources, Supervision. **Massimo Garai:** Funding acquisition. **Dario D'Orazio:** Writing – review & editing, Methodology, Supervision, Conceptualization.

Declaration of competing interest

The authors declare that they have no known competing financial interests or personal relationships that could have appeared to influence the work reported in this paper.

Data availability

Data will be made available on request.

References

[1] Yadav M, Cabrera D. Acoustic privacy. In: Routledge handbook of high-performance workplaces. Routledge; 2024. p. 102–15.
[2] Yadav M, Cabrera D, Kim J, Fels J, de Dear R. Sound in occupied open-plan offices: objective metrics with a review of historical perspectives. Appl Acoust 2021;177:107943.
[3] Pierrette M, Parizet E, Chevret P, Chatillon J. Noise effect on comfort in open-space offices: development of an assessment questionnaire. Ergonomics 2015;58(1):96–106.
[4] De Salvio D, D'Orazio D, Garai M. Unsupervised analysis of background noise sources in active offices. J Acoust Soc Am 2021;149(6):4049–60.
[5] Haapakangas A, Hongisto V, Eerola M, Kuusisto T. Distraction distance and perceived disturbance by noise — an analysis of 21 open-plan offices. J Acoust Soc Am 2017;141(1):127–36.
[6] De Salvio D, Fratoni G, D'Orazio D, Garai M, et al. Assessing human activity noise in workspaces using machine learning and numerical models. Noise-Con Proc 2023;265(2):5259–69.
[7] Golmohammadi R, Aliabadi M, Nezami T. An experimental study of acoustic comfort in open space banks based on speech intelligibility and noise annoyance measures. Arch Acoust 2017;42(2):333–45.
[8] Park SH, Lee PJ, Lee BK, Roskams M, Haynes BP. Associations between job satisfaction, job characteristics, and acoustic environment in open-plan offices. Appl Acoust 2020;168:107425.
[9] ISO 3382-3:2022 Acoustics – Measurement of room acoustic parameters.
[10] ISO 22955:2021 Acoustics – Acoustic quality of open office spaces.
[11] Kang S, Mak CM, Ou D, Zhang Y. The effect of room acoustic quality levels on work performance and perceptions in open-plan offices: a laboratory study. Appl Acoust 2022;201:109096.
[12] Moreland J. Role of the screen on speech privacy in open plan offices. Noise Control Eng J 1988;30(2):43–56.
[13] West M, Parkin P. Effect of furniture and boundary conditions on the sound attenuation in a landscaped office: Part 2—screens. Appl Acoust 1978;11(3):171–218.
[14] Fratoni G, De Salvio D, D'Orazio D. Virtual assessment of phone booths' acoustic performance in laboratory and office environments. Noise-Con Proc 2024;270(6):5668–75.
[15] Keränen J, Hakala J, Hongisto V. Effect of sound absorption and screen height on spatial decay of speech–experimental study in an open-plan office. Appl Acoust 2020;166:107340.
[16] Rindel JH. Attenuation of sound reflections due to diffraction. In: Proceedings of the nordic acoustical meeting, Aalborg, Denmark; 1986. p. 20–2.
[17] ISO 11654:1997 Acoustics — Sound absorbers for use in buildings — Rating of sound absorption.
[18] Brawata K, Baruch K, Kamisinski T, Chojnacki B. Transparent office screens based on microperforated foil. Audio engineering society convention, vol. 147. Audio Engineering Society; 2019.
[19] Keranen JS, Virjonen P, Hongisto VO. Characterization of acoustics in open offices-four case studies. Proc Acoust 2008:549–54.
[20] Sakagami K, Nakamori T, Morimoto M, Yairi M. Double-leaf microperforated panel space absorbers: a revised theory and detailed analysis. Appl Acoust 2009;70(5):703–9.
[21] Keränen J, Saarinen P, Hongisto V. Prediction accuracies of ray-tracing and regression models in open-plan offices. Build Environ 2023;239:110406.
[22] Braat-Eggen E, vd Poll MK, Hornikx M, Kohlrausch A. Auditory distraction in open-plan study environments: effects of background speech and reverberation time on a collaboration task. Appl Acoust 2019;154:148–60.
[23] Haapakangas A, Hongisto V, Hyönä J, Kokko J, Keränen J. Effects of unattended speech on performance and subjective distraction: the role of acoustic design in open-plan offices. Appl Acoust 2014;86:1–16.
[24] Schmich I, Rougier C, Jean P, Chevret P. Efficiency of an acoustic table screen between two work stations in open plan offices. In: Acoustics 2012; 2012.
[25] Balazova I, Clausen G, Rindel JH, Poulsen T, Wyon DP. Open-plan office environments: a laboratory experiment to examine the effect of office noise and temperature on human perception, comfort and office work performance. Indoor Air 2008;2008:17–22.
[26] Venetjoki N, Kaarlela-Tuomaala A, Keskinen E, Hongisto V. The effect of speech and speech intelligibility on task performance. Ergonomics 2006;49(11):1068–91.
[27] Wang C, Bradley J. A mathematical model for a single screen barrier in open-plan offices. Appl Acoust 2002;63(8):849–66.
[28] Wang C, Bradley J. Prediction of the speech intelligibility index behind a single screen in an open-plan office. Appl Acoust 2002;63(8):867–83.
[29] Pickett JM, Morris SR. The acoustics of speech communication: fundamentals, speech perception theory, and technology. Acoustical Society of America; 2000.
[30] Furui S. Digital speech processing: synthesis, and recognition. CRC Press; 2018.
[31] Cingolani M, Fusaro G, Fratoni G, Garai M. Influence of thermal deformations on sound absorption of three-dimensional printed metamaterials. J Acoust Soc Am 2022;151(6):3770–9.
[32] Huang S, Fang X, Wang X, Assouar B, Cheng Q, Li Y. Acoustic perfect absorbers via Helmholtz resonators with embedded apertures. J Acoust Soc Am 2019;145(1):254–62.
[33] Stinson MR, Shaw E. Acoustic impedance of small, circular orifices in thin plates. J Acoust Soc Am 1985;77(6):2039–42.
[34] Ingard U. On the theory and design of acoustic resonators. J Acoust Soc Am 1953;25(6):1037–61.
[35] ISO 9921:2003 Ergonomics — Assessment of speech communication.
[36] ISO 10534-2:1998 Acoustics — Determination of sound absorption coefficient and impedance in impedance tubes.
[37] COMSOL Multiphysics. Acoustics module user guide version 5.0. Users manual. Stockholm; 2014.
[38] Chen J-S, Chen Y-B, Cheng Y-H, Chou L-C. A sound absorption panel containing coiled Helmholtz resonators. Phys Lett A 2020;384(35):126887.
[39] Marburg S, Nolte B. Computational acoustics of noise propagation in fluids: finite and boundary element methods, vol. 578. Springer; 2008.
[40] Chung J, Blaser D. Transfer function method of measuring in-duct acoustic properties. i. theory. J Acoust Soc Am 1980;68(3):907–13.
[41] Chung J, Blaser D. Transfer function method of measuring in-duct acoustic properties. ii. experiment. J Acoust Soc Am 1980;68(3):914–21.
[42] Kim DH, Yoon GH. Active acoustic absorption device using additive manufacturing technique for normal incident wave. Appl Acoust 2021;178:108006.
[43] Boulvert J, Costa-Baptista J, Cavalieri T, Perna M, Fotsing ER, Romero-García V, et al. Acoustic modeling of micro-lattices obtained by additive manufacturing. Appl Acoust 2020;164:107244.
[44] Turner BN, Strong R, Gold SA. A review of melt extrusion additive manufacturing processes: I. process design and modeling. Rapid Prototyping J 2014;20(3):192–204.
[45] Fusaro G, Barbaresi L, Cingolani M, Garai M, Ida E, Prato A, et al. Investigation of the impact of additive manufacturing techniques on the acoustic performance of a coiled-up resonator. J Acoust Soc Am 2023;153(5):2921–31.
[46] Fratoni G, Tenpierik M, Turrin M, Garai M, D'Orazio D. Materials for the acoustic simulation of an open-plan office with desk screens to reduce speech distraction. Mendeley data. https://doi.org/10.17632/7kyj7wjdn7, 2024.
[47] D'Orazio D, Rossi E, Garai M. Comparison of different in situ measurements techniques of intelligibility in an open-plan office. Build Acoust 2018;25(2):111–22.
[48] Hamilton B, Webb CJ. Room acoustics modelling using gpu-accelerated finite difference and finite volume methods on a face-centered cubic grid. In: Proc Digital Audio Effects (DAFx), Maynooth, Ireland; 2013. p. 336–43.
[49] Pind F, Engsig-Karup AP, Jeong C-H, Hesthaven JS, Mejling MS, Strømann-Andersen J. Time domain room acoustic simulations using the spectral element method. J Acoust Soc Am 2019;145(6):3299–310.
[50] Lai H, Hamilton B. Computer modeling of barrel-vaulted sanctuary exhibiting flutter echo with comparison to measurements. Acoustics, vol. 2. Multidisciplinary Digital Publishing Institute; 2020. p. 87–109.
[51] Wang H, Hornikx M. Time-domain impedance boundary condition modeling with the discontinuous Galerkin method for room acoustics simulations. J Acoust Soc Am 2020;147(4):2534–46.
[52] Cingolani M, Fratoni G, Barbaresi L, D'Orazio D, Hamilton B, Garai M. A trial acoustic improvement in a lecture hall with MPP sound absorbers and FDTD acoustic simulations. Appl Sci 2021;11(6):2445.
[53] Fratoni G, Hamilton B, D'Orazio D. Feasibility of a finite-difference time-domain model in large-scale acoustic simulations. J Acoust Soc Am 2022;152(1):330–41.
[54] Fratoni G, D'Orazio D. Exploring sound diffusion in learning environments through experimental and wave-based analysis. Noise-Con Proc 2024;270(6):5641–8.
[55] Vorländer M. Auralization. Springer; 2020.
[56] Llopis HS, Kjær C, Engsig-Karup AP, Jeong C-H. Just noticeable difference for simulation accuracy between full and reduced order models (l). J Acoust Soc Am 2024;155(1):94–7.
[57] Pind F, Jeong C-H, Engsig-Karup AP, Hesthaven JS, Strømann-Andersen J. Time-domain room acoustic simulations with extended-reacting porous absorbers using the discontinuous Galerkin method. J Acoust Soc Am 2020;148(5):2851–63.
[58] Schroeder MR, Kuttruff K. On frequency response curves in rooms. comparison of experimental, theoretical, and Monte Carlo results for the average frequency spacing between maxima. J Acoust Soc Am 1962;34(1):76–80.
[59] Mondet B, Brunskog J, Jeong C-H, Rindel JH. From absorption to impedance: enhancing boundary conditions in room acoustic simulations. Appl Acoust 2020;157:106884.
[60] Fratoni G, D'Orazio D, Garai M. Uncertainty of input data for wave-based room acoustic simulations in large non-trivial environments. Proc Forum Acust 2023:123–30. https://doi.org/10.61782/fa.2023.1114.
[61] Vorländer M, Mommertz E. Definition and measurement of random-incidence scattering coefficients. Appl Acoust 2000;60(2):187–99.
[62] Pilch A. Optimization-based method for the calibration of geometrical acoustic models. Appl Acoust 2020;170:107495.
[63] Lenne L, Chevret P, Parizet E. Measurement uncertainty and unicity of single number quantities describing the spatial decay of speech level in open-plan offices. Appl Acoust 2021;182:108269.

[64] Yadav M, Cabrera D, Love J, Kim J, Holmes J, Caldwell H, et al. Reliability and repeatability of iso 3382-3 metrics based on repeated acoustic measurements in open-plan offices. Appl Acoust 2019;150:138–46.
[65] Lenne L, Aboutiman A, Selzer J, Schelle F, Chevret P, Parizet E. Simplified expressions of uncertainty for single number quantities in iso 3382-3 (2022). J Acoust Soc Am 2024;155(5):2909–18.
[66] Pan L, Martellotta F. A parametric study of the acoustic performance of resonant absorbers made of micro-perforated membranes and perforated panels. Appl Sci 2020;10(5):1581.